JCTC Journal of Chemical Theory and Computation

Article

pubs.acs.org/JCTC

Decrypting Prion Protein Conversion into a β-Rich Conformer by Molecular Dynamics

Nesrine Chakroun,[†,‡] Arianna Fornili,[‡] Stéphanie Prigent,[§] Jens Kleinjung,[∥] Cécile A. Dreiss,[†] Human Rezaei,[§] and Franca Fraternali*[,†,⊥]

[†]Institute of Pharmaceutical Science, King's College London, 150 Stamford Street, London, SE1 9NH, United Kingdom

[‡]Randall Division of Cell and Molecular Biophysics, King's College London, Guy's Campus, London, SE1 1UL, United Kingdom

[§]Institut National de la Recherche Agronomique (INRA), Virologie et Immunologie Moléculaires, Equipe Biologie Physico-chimique des Prions, Jouy-en-Josas, France

[∥]Division of Mathematical Biology, MRC National Institute for Medical Research, Mill Hill, London, NW7 1AA, United Kingdom

[⊥]The Thomas Young Centre for Theory and Simulation of Materials, London, United Kingdom

Supporting Information

ABSTRACT: Prion diseases are fatal neurodegenerative diseases characterized by the formation of β-rich oligomers and the accumulation of amyloid fibrillar deposits in the central nervous system. Understanding the conversion of the cellular prion protein into its β-rich polymeric conformers is fundamental to tackling the early stages of the development of prion diseases. In this paper, we have identified unfolding and refolding steps critical to the conversion into a β-rich conformer for different constructs of the ovine prion protein by molecular dynamics simulations. By combining our results with *in vitro* experiments, we show that the folded C-terminus of the ovine prion protein is able to recurrently undergo a drastic conformational change by displacement of the H1 helix, uncovering of the H2H3 domain, and formation of persistent β-sheets between H2 and H3 residues. The observed β-sheets refold toward the C-terminus exposing what we call a "bending region" comprising residues 204−214. This is strikingly coincident with the region harboring mutations determining the fate of the prion oligomerization process. The β-rich intermediate is used here for the construction of a putative model for the assembly into an oligomeric aggregate. The results presented here confirm the importance of the H2H3 domain for prion oligomer formation and therefore its potential use as molecular target in the design of novel prion inhibitors.

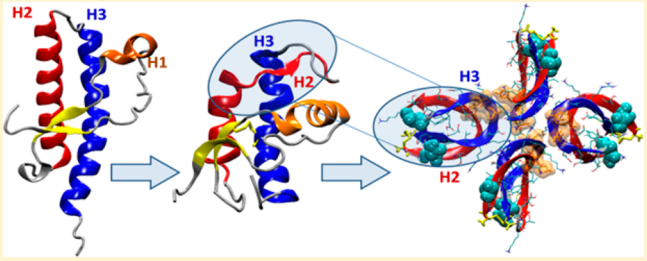

INTRODUCTION

Transmissible spongiform encephalopathies or prion diseases are fatal transmissible neurodegenerative disorders affecting a wide range of mammals: Creutzfeldt−Jakob disease in humans and bovine spongiform encephalopathy and Scrapie, affecting cattle and sheep, respectively. Prion diseases are usually characterized by brain vacuolation, neuronal apoptosis, and/or the accumulation of extracellular amyloid plaques in the central nervous system. According to the protein-only or "prion" hypothesis,[1] the key event in the pathogenesis is the conversion of the α-helix-rich cellular prion protein (PrP^C) into its polymeric β-sheet rich isoform PrP^{Sc}. While PrP^C has been widely studied, PrP^{Sc} is still poorly characterized, and the molecular determinants in the conversion process of PrP^C into PrP^{Sc} are unclear. PrP^C is associated to the outer-cell membrane by a glycosyl phospho-inositol anchor through its C-terminus.[2] It has a flexible and unstructured N-terminus and a globular C-terminus comprising two native β-sheets S1 and S2 and three α-helices H1, H2, and H3[3] (Figure 1A). PrP^{Sc}, which is polymeric, heterogeneous in terms of quaternary structure and enriched in β-sheets, is difficult to purify in quantities high enough for structural characterization. The possibility of working with *in vitro* models of the recombinant PrP has provided precious clues on the fibrillation and oligomerization processes.[1,4] Several studies have highlighted the amyloidogenic and cytotoxic properties of the N-terminus region;[5] therefore the implication of the N-terminus and S1H1S2 must also be taken into account in determining the cytotoxic effects of PrP amyloid fibrils. Shmerling et al.[6] have shown that N-terminally truncated PrP (PrPΔ32−134) was able to induce cerebellar degeneration in PrP deficient mice, suggesting that the N-terminus may not be critical for prion replication. The potential role of H2 and H3 in the α to β conversion of PrP was first suggested by Dima and Thirumalai[7] in their computational analysis of available NMR structures of PrP. Tycko et al.[4c] used solid state NMR on fibrils formed by hamster PrP and showed that the C-terminal end forms the structurally ordered core of the fibrils. The critical role of the region formed by H2 and H3 (in ovine recombinant PrP) in the formation of oligomers *in*

Received: December 21, 2012
Published: April 4, 2013

   dx.doi.org/10.1021/ct301118j | J. Chem. Theory Comput. 2013, 9, 2455−2465

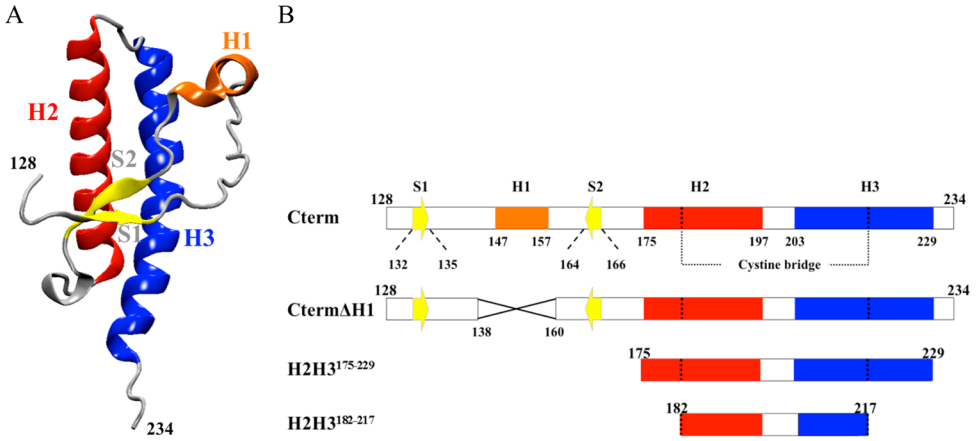

Figure 1. OvPrP constructs and MD simulation scheme. (A) 3D structure of the Cterm$^{128-234}$ region of OvPrP showing helices H1 (orange), H2 (red), and H3 (blue) and native β-sheets S1 and S2 (yellow). (B) OvPrP constructs used in the oligomerization analysis and MD simulations.

vitro has recently been demonstrated.[4b] The globular region comprising the H2H3 domain has also been shown by NMR to be an independent α-helical unit that is able to form fibrils.[4a] Recently, the H2H3 region was shown to undergo glycosyl phospho-inositol anchoring in cells, similarly to the full length PrP, and to undergo a conversion process with the generation of insoluble PK-resistant aggregates.[8]

Molecular dynamics (MD) simulations have been increasingly used in the prion field to provide an atomistic understanding of the protein's unfolding.[4b,9] DeMarco and Daggett[10] have shown that glycosylation and membrane anchoring do not significantly alter the *in silico* structure and/or dynamics of PrP^{C}, thereby affirming the choice of the globular region for prion simulations. The effects of pH[11] and temperature[12] and the combination of both[9a] on the stability and dynamics of human PrP^{C} have been widely investigated. Langella et al.[11] observed that under mildly acidic conditions a significant loss of α-helix content occurs within H2 of the human PrP^{C}. Colacino et al.[12a] and Blinov et al.[12b] reported that at high temperatures, H2 unfolds first, followed by H3. It has also been observed that at low pH and high temperatures H2 is the most unstable secondary structure in human PrP^{C}.[9a] Coarse-grained MD simulations of the CJD-causing T183A variant have demonstrated that the H2H3 subdomain has a high propensity for intra- and intermolecular β-sheet formation.[13] De Simone et al.[14] investigated the C-terminal domain of human PrP using replica exchange MD simulations. They observed a stable core formed by the H2H3 domain and a higher mobility of H1. An analogous behavior was observed by van der Kamp and Daggett[15] in the wild type (WT) and some disease-associated mutants of the human PrP (90−230), specifically a displacement of H1 and an instability of the hydrophobic core, which is formed by 20 residues packed between H2, H3, and H1.[3]

By focusing only on the H2H3 domain, we observed *in silico* a complete conversion from an all-helical structure to a stable β-rich intermediate.[4b] Our MD simulations, together with experimental evidence, have confirmed that the early stage oligomer formation can be ascribed solely to the H2H3 region and does not involve the native β-sheets present in the folded PrP^{C} domain as previously suggested.[16] These observations have important implications for the assembly mechanism of the early oligomeric intermediates.

In this work, we have performed in total 5.7 μs of MD simulations on a range of constructs of the ovine PrP (OvPrP) at pH 3.3 and high temperatures. Our intent was to obtain a detailed understanding of the mechanism enabling the conversion from the full-length PrP^{C} to a β-rich conformer contributing to the PrP^{Sc} state and testing its reproducibility and the implications of such an intermediate in the assembly of PrP^{Sc} oligomers. In this work, simulation of the folded OvPrP(128−234) was carried out for 1 μs, yielding, also in this case, through drastic conformational changes, to the formation of a β-sheet rich conformer. We extended the analysis to various constructs of OvPrP that were shown experimentally to follow an oligomerization pattern similar to the full length PrP. Overall, our approach of combining oligomerization profiling by size exclusion chromatography with MD simulations reveals a common scheme of unfolding and refolding of specific regions of the PrP leading to the conversion of the α-rich PrP (PrP^{C}) into a range of β-rich conformers.

MATERIALS AND METHODS

Protein Production and Size Exclusion Chromatography. The full-length recombinant A136R154Q171 WT variant OvPrP was produced and purified according to the previously described protocol.[17] The CtermΔH1(147−157), OvPrPI206A, and OvPrPI208A constructs were cloned into pET 28 vector and purified by recovering the inclusion bodies into 6 M guanidine HCl containing 10 mM imidazol, pH 7.1. The supernatant containing the unfolded OvPrP domains was loaded into a Ni-NTA column. A washing step with a buffer without a chaotropic agent leads to the heterogeneous phase refolding of attached OvPrP domains. Samples were desalted using ammonium acetate (0.5 g/L, pH 5.0) and freeze-dried. The generation of OvPrP oligomers and their analysis by size exclusion chromatography were performed as described previously.[17]

Preparation of Starting Structures for MD Simulations. All starting structures for MD (Figure 1A and B) were modeled from the crystal structure of the globular domain of the OvPrP (PDB 1UW3).[18] The OvPrP C-terminal construct Cterm$^{128-234}$ contains residues 128−234, while CtermΔH1 was depleted of H1 residues 138−160. Shorter constructs spanning residues from H2 and H3 only were used: H2H3$^{175-229}$ spanning residues 175−229 and H2H3$^{182-217}$ spanning residues

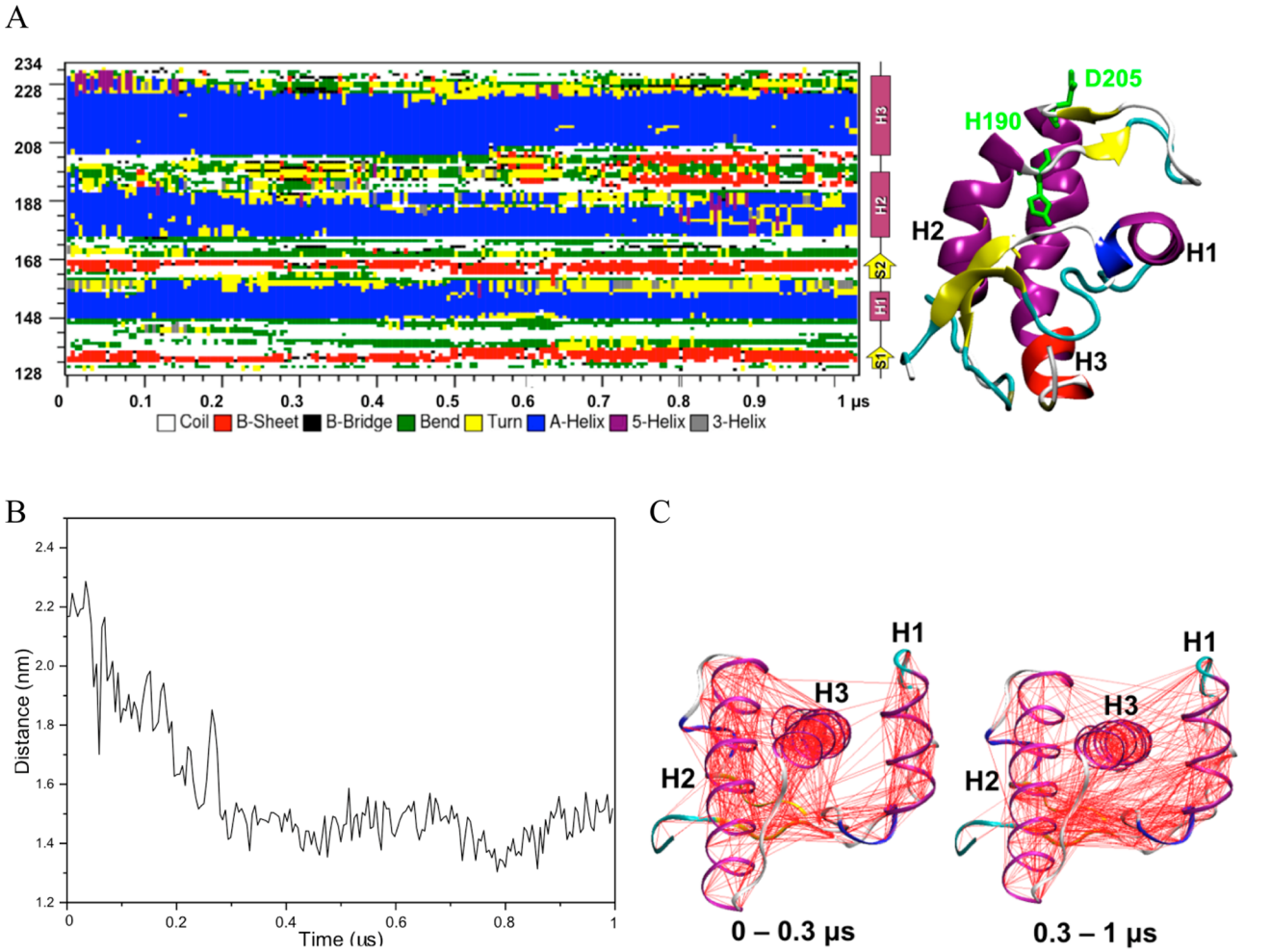

Figure 2. Simulation of Cterm$^{128-234}$. (A) Left panel: Evolution of the secondary structure of Cterm$^{128-234}$ at 338 K (65 °C). The *x* axis represents the simulation time and the *y* axis the peptide sequence, colored by secondary structure type, over the simulation time. The simulation at 338 K included a 30 ns heating protocol at 328 K (55 °C; heating rate 5.6 K/ns) followed by heating to 338 at 4 K/ns. Right panel: 1 μs frame of Cterm$^{128-234}$ showing the partial unfolding of H2 and H3 and the formation of a β-sheet. (B) Distance evolution between the native disulfide bridge and H1 highlighting the displacement of H1 toward the C-terminus of OvPrP. (C) Correlated motions calculated for C$^{\alpha}$; a line is drawn between each atom with a "per atom normalized covariance" > 30%.

182−217. H2H3$^{182-217}$I206A and H2H3$^{182-217}$I208A include additionally mutations I206A and I208A, respectively.

MD Simulations. MD simulations were carried out using the GROMACS package[19] with the GROMOS96 43a1[20] and the recent GROMOS 53a6[21] force fields. The PME method was used for the calculation of electrostatic contributions to the nonbonded interactions.[22] Structures were solvated with SPC water molecules[23] and Cl^- as counterions. Periodic boundary conditions were applied. The Berendsen algorithm[24] was used for temperature and pressure coupling.

The simulations were carried out at high temperatures (338 K) and low pH (pH 3.4), reproducing *in vitro* experimental conditions that aim at enhancing the conversion rate. Cterm$^{128-234}$ was simulated for 1 μs, and its 700 ns frame was used as a starting structure for the simulations of CtermΔH1, H2H3$^{175-229}$ (simulation labeled as H2H3$^{175-229}$-1), and H2H3$^{182-217}$ (Figure S1 in the Supporting Information). Cterm$^{128-234}$ was also simulated for 500 ns by restraining the distances between residues Asp144, Tyr149, and Met154 from H1 to the disulfide bridge (labeled as Cterm$^{128-234\text{-restr}}$). A control simulation of the segment 128−174 corresponding to the S1H1S2 region was carried out in two replicas. We also performed replica simulations of H2H3$^{175-229}$ (labeled as H2H3$^{175-229}$-2) and H2H3$^{182-217}$ starting from the PDB structure 1UW3.

Analysis of MD Trajectories of Prion. MD trajectories were analyzed using the GROMACS package; secondary structure content was determined using DSSP.[25] Correlated motions were analyzed with Dynamite.[26] Surface accessible areas were calculated using the GROMACS package and the POPS program.[27]

Analysis of Water Density around the Constructs. For the purpose of water density analysis, structures were simulated, as previously described, for 5 ns by MD with backbone restraints (1.2 kcal·mol^{-1}·Å^{-2}) to avoid any significant conformational changes of the protein during the simulation.[28] Water distribution analysis was performed around representative conformations of the H2H3$^{182-217}$I206A and H2H3$^{182-217}$I208A trajectories and compared to the solvent distribution previously obtained for the wild-type H2H3$^{182-217}$ conformation with the highest content of β-strands.[28] The structures were extracted using the Daura algorithm for clustering implemented in Gromacs[29] with a 3.3 Å cutoff and by selecting representative structures from the most populated

dx.doi.org/10.1021/ct301118j | J. Chem. Theory Comput. 2013, 9, 2455−2465

Table 1. Secondary Structure Analysis of Cterm$^{128-234}$, CtermΔH1, H2H3$^{175-229}$-1, H2H3$^{175-229}$-2, and H2H3$^{182-217}$ Simulations[a]

	Cterm$^{128-234}$			CtermΔH1			H2H3$^{175-229}$-1			H2H3$^{175-229}$-2			H2H3$^{182-217}$		
secondary structure content	start	end	change	start	end	change	start	end	change	start	end	change	start	end	change
total (%)	65	57	−8	38	42	+4	45	29	−16	45	17	−28	14	18	+4
β-conformation (%)	4	11	+7	0	11	+11	0	6	+6	0	6	+6	0	11	+11
helical conformation (%)	68	38	−30	28	31	+3	43	22	−21	43	11	−32	14	5	−9
R_g (nm)	1.50	1.33	−11%	1.25	1.21	−3%	1.26	1.04	−17%	1.36	1.03	−24%	0.99	0.89	−10%
	H2H3$^{182-217}$I206A			H2H3$^{182-217}$I208A			H2H3$^{182-217}$ replica 1			H2H3$^{182-217}$ replica 2			H2H3$^{182-217}$ replica 3		
secondary structure content	start	end	change	start	end	change	start	end	change	start	end	change	start	end	change
total (%)	29	21	−8	26	15	−11	30	17	−13	30	16	−14	30	13	−17
β-conformation (%)	0	7	+7	0	1	+1	0	15	+15	0	11	+11	0	2	+2
helical conformation (%)	28	10	−18	23	5	−18	28	0	−28	28	3	−25	28	9	−19
R_g (nm)	0.96	0.86	−10%	0.96	0.86	−10%	1.00	0.93	−6%	1.00	0.91	−9%.	1.00	0.87	−13%

[a]start, starting structure; end, averaged over the last 50 ns, except for H2H3$^{175-229}$-1 averaged over the last 20 ns.

cluster. Briefly, the water density function $g(\mathbf{r})$[30] was calculated at discrete positions $\mathbf{r}$ defined by a 0.5 Å spaced rectangular grid around the solute. The maxima of the $g(\mathbf{r})$ distribution were used to define the atomic hydration score S_{hyd}^{atom} and the residue hydrophobicity score S_{phob}^{res} as previously described.[28]

Assembly. Molecular models of oligomers were assembled by rigid body transformation of replicas of a given initial structure, e.g. a tetramer obtained by docking using ZDOCK[31] and further minimized by steepest descent in GROMACS. The initial structure was first oriented relative to a symmetry axis (here the "z" axis) such that putative interaction surfaces would face each other in the oligomer. The following spatial transformation operations were performed on each replica of the oriented initial structure: (i) translation by a given distance "d_{xy}" orthogonal to the symmetry axis, (ii) rotation by a given angle "φ" around the symmetry axis, and (iii) translation by distance d_z parallel to the symmetry axis. The distances "d_{xy}" and "d_z" were chosen such that the replicas were in close contact without clashes. The angle "φ" was set to 90° to create a 4-fold symmetry around the "z" axis.

RESULTS

We present here the simulations performed on the different constructs shown in Figure 1B. A summary of the simulations is presented in Figure S1. Most constructs were run for 300 ns; for Cterm$^{128-234}$ however, a longer simulation time (1 μs) was needed to monitor the effects of the observed conformational changes. It is important to note that some of the simulations were carried out as replicates with different initial velocities (starting structures), and the observed convergence gives us confidence in the results presented below.

First Step in the Conversion: Opening of the Folded Domain. The simulation of Cterm$^{128-234}$ (Figure 1) was carried out for a total of 1 μs at 338 K. The secondary structure assignment (DSSP) to the trajectory is shown in Figure 2A. One can distinguish two main phases in the unfolding process: (i) the unfolding of residues Thr186−Lys197 of H2 during the first 540 ns, followed by (ii) the unfolding of residues Glu203−Lys207 of H3 and the formation of a β-sheet between residues Thr191−Lys197 and Glu199−Thr204 (Figure 2A, left). Table 1 compares the secondary structures content between the start and end conformations and shows that the helical structure content drops from 68% to 38% in Cterm$^{128-234}$, while the β-structure content increases by 7%. The radius of gyration (R_g) decreases by 11% (Table 1), showing a more compact structure after 1 μs of simulation. Strong conformational fluctuations with major rearrangements are observed within H1 (residues 147−157) during the first 300 ns of the simulation: starting at a conformation in which H1 faces residue Thr204 of H3, H1 ends up facing residue Met216 of H3 after 300 ns (Figure 2A, right). This is well illustrated by following the distance between the center of mass of H1 (residues 147−156) and the native Cys182−Cys217 bridge: they are 2.2 nm apart in the starting structure; then the distance gradually decreases to 1.4 nm (± 0.1 nm) over the first 300 ns, after which it stabilizes until the end of the simulation (Figure 2B). The dynamics of the protein was analyzed in terms of correlated motions, and the covariance of pairs of C^{α} coordinates was calculated using Dynamite. During the first 300 ns, when the major displacement of H1 occurs, residues in H1 show a relatively independent motion from the rest of the protein as shown by the correlated motion plot (Figure 2C). Conversely, from 300 ns to the end of the simulation, the motions between H1 and the rest of the protein are highly correlated (Figure 2C).

The distance between Lys197 at the extremity of H2 and Cys217 was calculated during the simulation, as in our previous work,[4b] monitoring the unfolding of H2 (as the distance increases) and the refolding toward the C-terminus (distance decreases to a value smaller than at the start; Figure S2A). The Lys197−Cys217 distance oscillates strongly between 2.8 and 1.4 nm during the simulated trajectory, revealing the unfolding of H2 residues Thr186−Lys197 and the partial refolding of the β-sheet toward the C-terminus. The bending of the structure is located at residues H2−His190 and H3−Asp205 (Figure 2A, right). Because this refolding occurs at the time when H1 is displaced, we followed the formation of hydrogen bonds between H1 and the initial loop between H2 and H3. We observed an average of 0.8 hydrogen bonds during the first 600 ns and 2.2 during the last 400 ns (Figure S2A). This shows that H1 becomes hydrogen-bonded to residues initially forming the loop between H2 and H3 and therefore may be obstructing the bending that leads to its refolding toward the C-terminus. A displacement of the native β-sheet S2 (residues 164−166) from the core of the protein was also observed: initially 0.5 nm apart, the distance between the center of mass of S2 and Cys182 increases to 1 nm (Figure S2A). The start and end energies of

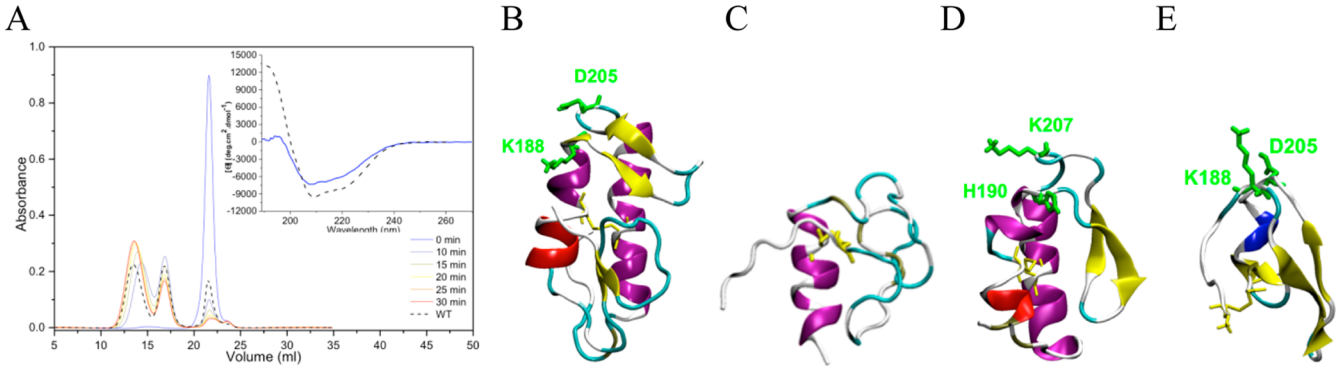

Figure 3. Simulations of various OvPrP constructs. (A) Size-exclusion chromatogram of CtermΔ147−157 (blue to red polymerization at 80 μM at 50 °C (0−30 min) and pH 3.4). OvPrP at 80 μM, 30 min, 50 °C is shown as reference (dashed line). Inset: CD spectra of CtermΔ147−157 (blue) and OvPrP (dashed line). (B) Cartoon representation of the 300 ns conformation of the CtermΔH1 simulation at 338 K. (C) Cartoon representation of the 200 ns frame of H2H3$^{175-229}$-2 at 338 K starting from the 700 ns conformation of the simulation of Cterm$^{128-234}$. (D) Cartoon representation of the 400 ns conformation of H2H3$^{175-229}$-1 at 338 K starting from the crystal structure of OvPrP; residues where bending occurs are shown in green. (E) Cartoon representation of the 700 ns conformation of H2H3$^{182-217}$ at 338 K starting from the 700 ns conformation of the simulation of Cterm$^{128-234}$; residues where bending occurs are shown in green.

the simulated constructs, averaged over 50 ns (Figure S3), show a correlated trend with the radius of gyration. A lowering of the R_g generally corresponds to a more favorable intraprotein potential energy at the expense of solvent−protein energy contributions.

Is H1 Structurally Obstructing the Unfolding of H2 and H3? In order to test the hypothesis that H1 might act as a barrier to the unfolding of H2 and H3, we designed a construct in which H1 was deleted. Experimentally, this construct shows a similar oligomerization profile to the full-length OvPrP, therefore strongly supporting the hypothesis that the presence of H1 is unessential to the oligomerization process of OvPrP^{C} (Figure 3A). A similar construct CtermΔH1 was simulated for 300 ns under the same conditions as Cterm$^{128-234}$, starting from the 700 ns frame of the Cterm$^{128-234}$ simulation. We observed the persistence of a β-sheet between the stretches of residues Gln185−Thr195 and Gly198−Glu203 (Figure 3B and Table 1). The bending was located at residues H2−Lys188 and H3−Asp205(Figure 3B). The displacement of H2H3 (Thr191−Thr204) toward the C-terminus observed during the simulation of Cterm$^{128-234}$ was also visible in CtermΔH1, as illustrated by the distance between Lys197 and Cys217, which decreases slightly from 2 to 1.8 nm (Figure S2B) and by a slight decrease of the R_g of about 3% (Table 1). Again, as observed in the Cterm$^{128-234}$ simulation, the distance between the center of mass of native S2 and Cys182 increases slowly from 0.7 to 1.1 nm, showing the displacement of S2 from the core of the protein (Figure S2 A).

To confirm the role of H1 in the Cterm$^{128-234}$ conversion, a 500 ns simulation of Cterm$^{128-234}$ was carried out, in which the distances between H1 and the disulfide bridge were restrained (Figure S4A). We observed minor structural changes such as a slight decrease in helical content (−6%) mainly in H2, while H1 and H3 were stable. Nonpersistent β-bridges were observed between residues Val192−Thr193 and Glu199−Asn200, and R_g remained unchanged at a value of 1.43 nm. Unlike the Cterm$^{128-234}$ simulation, we did not observe the refolding of H2 and H3 into a β-rich conformer when the position of H1 was restrained.

A Repeatedly Observed α to β Conversion: A Common Mechanism of Unfolding. Here, we focus on the region spanning H2 and H3 (Figure 1B), which we previously showed to be critical for the oligomerization behavior of OvPrP.[4a,b] H2H3 was also shown to form similar fibrils to those formed by OvPrP.[4a] The displacement of S2 from the core of OvPrP in the simulations of Cterm$^{128-234}$ and CtermΔH1 indicates that H2H3 may need to be uncovered and exposed to enable the conversion to the β-rich state as previously suggested.[4b,32]

WT H2H3$^{175-229}$. We tested *in silico* this mechanistic hypothesis by performing simulations of a shorter OvPrP$^{175-229}$ construct spanning residues 175−229 only (Figure 1B). The simulation was carried out in two replicas with different starting structures: one starting from the 700 ns frame of the Cterm$^{128-234}$ simulation by keeping residues 175−229 only (H2H3$^{175-229}$-1) and the other from the crystal structure PDB 1UW3 referred to as H2H3$^{175-229}$-2 (Figure S1). A control simulation of the peptide S1H1S2 (residues 128−174) was also carried out in two replicas for 200 ns each, in which we did not observe any *de novo* β-sheet formation (Figure S4B).

In the H2H3$^{175-229}$-1 simulation (200 ns), the unfolding of H2 and the partial unfolding of H3 was again observed (Figure 3C). Although residues Glu213−Tyr229 of H3 do not unfold, the whole structure refolds into a hairpin, illustrated by the decrease of the R_g by 18% (Table 1). In the H2H3$^{175-229}$-2 simulation (400 ns), the unfolding of H2 residues 188−197 and residues 203−211 of H3 occurred. We also observed the formation of sporadic β-bridges between the segments Gly192−Asp197 (H2) and Tyr199−Asn203 (H3). The unfolding of H2 and H3 residues is accompanied by the refolding of the structure into a hairpin with bending located at residues H2−His190 and H3−Lys207 (Figure 3D and Table 1). In both H2H3$^{175-229}$ simulations, we observe strong hydrogen bonding between Asp181 and Ile185 and between Met216 and Gln220, stabilizing the helical structure of H2 and H3. The simulations show the formation of *de novo* β-structures (+6% in both simulations) and the loss of helical structure content (−21% in H2H3$^{175-229}$-1, −32% in H2H3$^{175-229}$-2; Table 1).

Getting Shorter: H2H3$^{182-217}$. We had previously simulated the construct H2H3$^{182-217}$ under similar conditions, starting from the crystal structure, and observed its refolding into a β-rich double hairpin.[4b] In order to reinforce these observations, we replicated the simulation using a different start

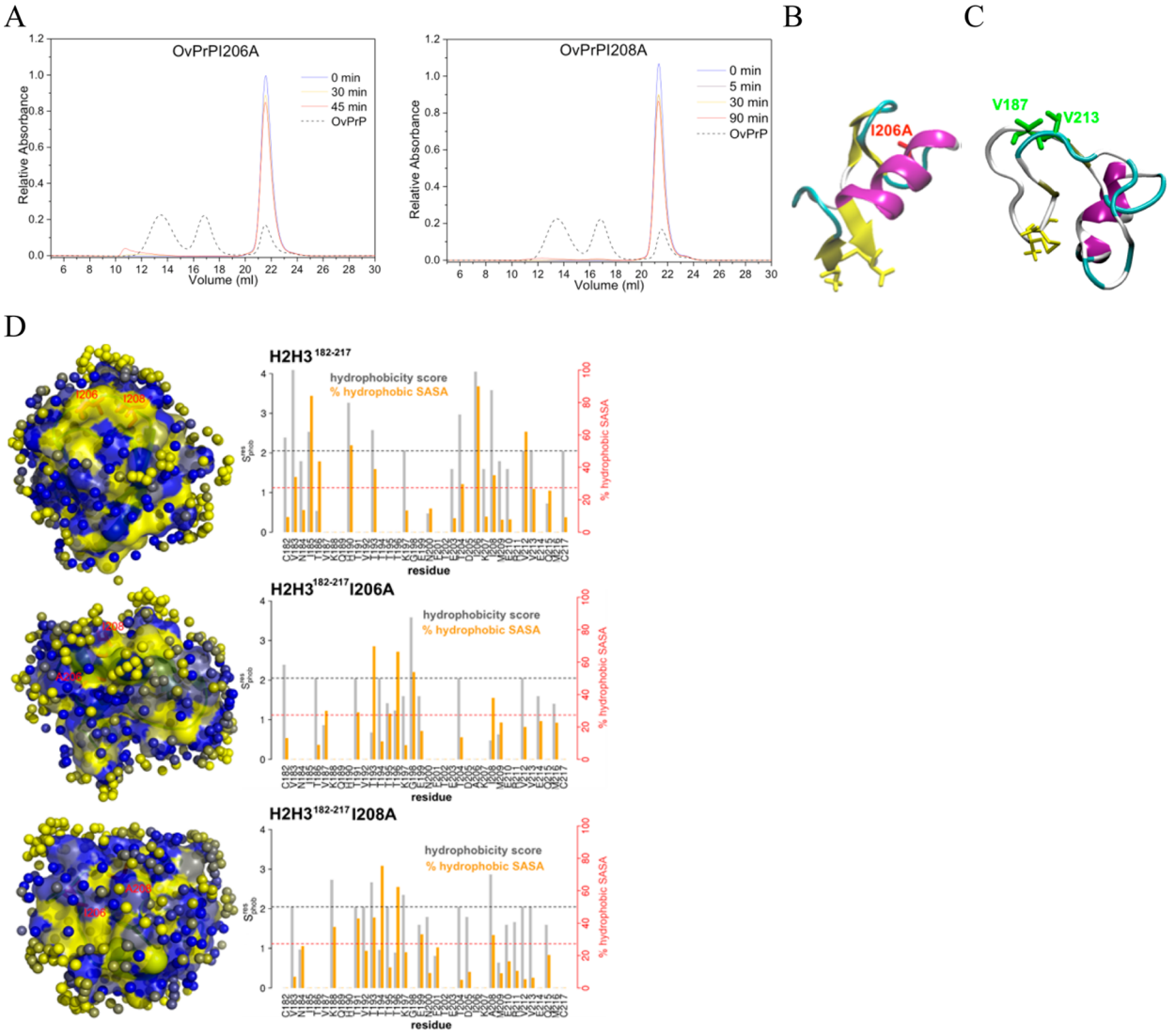

Figure 4. Effect of the I206A and I208A point mutations on the oligomerization of OvPrP at 80 μM, 30 min, 50 °C, pH 3.4. (A) Size-exclusion chromatogram of the oligomerization of OvPrPI206A (left) and OvPrPI208A (right). OvPrPI206A (blue and red lines) and OvPrP (dashed line) and OvPrPI208A (blue and red lines) and OvPrP (dashed line). (B) Cartoon representation of the 500 ns conformation of the H2H3$^{182-217}$I206A simulation at 338 K. (C) Cartoon representation of the 500 ns conformation of the H2H3$^{182-217}$I208A simulation at 338 K; residues where bending occurs are shown in green. (D) 3D maps of the atomic hydration score S_{hyd}^{atom} (left panels) and profiles of surface hydrophobicity scores S_{phob}^{res} (right panels) of H2H3$^{182-217}$ (top), H2H3$^{182-217}$I206A (middle), and H2H3$^{182-217}$I208A (bottom). Surface atoms are colored from yellow (low hydration) to blue (high hydration). Each structure is oriented such that the I/A residues 206 and 208 are visible together with their environment. The maxima of the water density function[28] are reported as spheres, colored from yellow (low density) to blue (high density). In the right panels, the per residue surface hydrophobicity score S_{phob}^{res} and relative hydrophobic SASA are reported. The black and red dashed lines mark the third quartile (highest 25% of values) of the WT S_{phob}^{res} and relative SASA distributions, respectively.

conformation. We used again the 700 ns frame of the Cterm$^{128-234}$ simulation as a start structure but kept only residues 182−21 and followed the conformational changes for a further 700 ns. We observed the complete unfolding of the H2 and H3 helices and the refolding into a β-hairpin in accordance with previous findings,[4b] paralleled by an 11% decrease of the R_g (Figure 3E and Table 1). The absence of Ile185 (H2) and Gln220 (H3) residues, and thus the absence of hydrogen bonds with Asp181 (H2) and Met216 (H3) (as observed in H2H3$^{182-217}$ simulations), weakens the helical fold of H2 and H3. Persistent β-bridges were also formed between stretches Thr194−Glu199 and Phe201−Asp205 during the last 600 ns of the simulation, yielding an increase of 11% in β-structure content (Table 1).

Additionally, we performed three replica simulations starting from the crystal structure of H2H3$^{182-217}$. Two of the replicas (replica 1 and 2) showed the complete unfolding of the helices with stable β-sheet formation, while the third replica partially unfolded and a β-seed was formed, as previously observed[4b] (Table 1 and Figure S4). The similarities between replica 1 and 2 are reflected in the values of their respective R_g (Table 1) and in the calculated relative energy contributions (Figure S3). We tested on this construct putative force-field dependence of the β-sheet conversion. A 22 ns simulation of H2H3$^{182-217}$ with the GROMOS 53a6 force field showed again the complete unfolding of the α-helical structures and the formation of a β-rich configuration (Figure S4). Residues 193−195 (H2), 215−217 (H3), 200−203 (H2) and 206−209 (H3) were involved in the β-structures, as observed in all our 43a1 force

field simulations. Although the pairing of β-strands was not identical to the double β-hairpin conformer in the previous simulations, it supports the high propensity of H2H3 to unfold and to convert into a β-rich conformer observed in all of our 43a1 force field simulations.

With the purpose of identifying residues playing a critical role in the oligomerization of OvPrP, we performed alanine mutagenesis on several residues. This approach allowed the identification of a number of residues that significantly affected the oligomerization pathway. As shown in Figure 4A, the mutations I206A (H3) and I208A (H3) prevent oligomerization *in vitro*. Therefore, we simulated both constructs, $H2H3^{182-217}$I206A and $H2H3^{182-217}$I208A, under the same conditions as the WT constructs (Figure S1).

Mutation Effects in the Hinge Region. *$H2H3^{182-217}$I206A.* As observed in the simulations of the WT constructs ($Cterm^{128-234}$, CtermΔH1, and $H2H3^{175-229}$), the 500 ns trajectory of $H2H3^{182-217}$I206A shows a rapid unfolding of H2 (residues 183−199) and a partial unfolding of H3 (residues 214−215) (Figure 4B). A β-seed is formed between stretches Val183−Asn184 and Gln214−Met215 after 60 ns and remains stable until the end of the simulation. β-bridges are also formed around 430 ns between stretches Thr196−Gly198 and Thr204−Ile206. Differently from the simulation of $H2H3^{182-217}$, H3 did not unfold completely within the simulation time (Table 1). In particular, Ala206 and Glu210 shared a strong and persistent hydrogen bond, thus preventing H3 from unfolding (Figure S6). Ala residues present indeed a higher conformational preference for α-helix compared to Ile residues,[33] and this could explain the persistence of a folded H3 in this construct.

$H2H3^{182-217}$I208A. The 500 ns simulation of $H2H3^{182-217}$I208A showed a partial unfolding of both H2 and H3 during the first 450 ns and their complete unfolding within the last 50 ns (Figure 4C and Table 1). We did not observe any β-sheet formation within the $H2H3^{182-217}$I208A construct; however, the structure refolded into a hairpin with bending occurring at Val187 in H2 and Val213 in H3 (Figure 4C). Quite remarkably, in the last 150 ns we observed helix formation by residues Gly198 to Glu203, which were originally part of the loop between H2 and H3.

We note that the refolding of the H2H3 loop toward the C-terminus was observed in all WT simulations and in the $H2H3^{182-217}$I208A mutant. The region where the bending is located is very similar in all WT constructs: H2 Lys188−His190 and H3 Asp205−Lys207 (Figures 2A and 3B−E). Instead, the bending in the $H2H3^{182-217}$I208A mutant occurs at residues H2 Val187 and H3 Val213 (Figure 4C). The bending occurred at residues His190 and Lys207 in our previous simulations of $H2H3^{182-217}$.[4b]

Water Analysis: Hydrophobicity Revisited and Implications for Assembly. Hydration maps around the mutants $H2H3^{182-217}$I206A and $H2H3^{182-217}$I208A were created by calculating the water density distributions of representative conformations extracted from the respective MD trajectories (see Materials and Methods). The results were compared with the hydration maps calculated for the WT construct $H2H3^{182-217}$.[28] The WT conformation presents the highest total (2630 Å^2) and hydrophobic (1529 Å^2) solvent accessible surface area (SASA) as evaluated by the POPS program (Table 2). A reduction by 220 Å^2 and 188 Å^2 in the total SASA was observed for $H2H3^{182-217}$I206A and $H2H3^{182-217}$I208A, respectively, and a corresponding decrease of 18 Å^2 and 89 Å^2 in the hydrophobic SASA. The comparison of the hydration scores S_{hyd}, derived from the maxima of the water density distribution, highlights significant differences in the water distribution around the mutated residues I206 and I208 (Figure 4D, left panels). In $H2H3^{182-217}$, these two residues are part of an extended hydrophobic patch (Figure 4D, upper panels). However, when either of them is mutated to alanine, a more hydrophilic local environment is observed around this region (Figure 4D, middle and lower panels). Correspondingly, the surface hydrophobicity scores of these residues are significantly reduced in both mutants (Figure 4D, right, middle, and lower panels) with respect to the WT (Figure 4D, right upper panel). Overall, the hydration maps and the hydrophobicity calculations enabled the identification of two patches within $H2H3^{182-217}$ that could potentially act as nuclei of fibrillation and oligomerization. The first patch comprises H2 residues Val183, Asn184, and Ile185; the second covers the H3 region Ile206−Val212.

Table 2. Solvent Accessible Surface Areas (SASA)[a]

SASA (Å^2)	$H2H3^{182-217}$	$H2H3^{182-217}$I206A	$H2H3^{182-217}$I208A
total	2630	2410	2442
hydrophobic	1529	1511	1440

[a]Total and hydrophobic SASA (in Å^2) as given by the POPS program of $H2H3^{182-217}$, $H2H3^{182-217}$I206A, and $H2H3^{182-217}$I208A.

DISCUSSION

In the present paper, we have combined MD simulations with experimental oligomerization studies of several tailor-made $OvPrP^C$ constructs to investigate the structural and dynamic changes of $OvPrP^C$ that may lead to its conversion into the β-rich $OvPrP^{Sc}$ form.

Critical Steps toward PrP^{Sc} Conversion. As previously reported,[34] the truncated OvPrP(104−234), spanning the structured C-terminal region of the OvPrP, follows a similar oligomerization pattern as the full-length OvPrP. The simulation of the globular region of OvPrP(128−234) ($Cterm^{128-234}$), at 338 K and low pH, revealed the unfolding of H2 residues 186−197 and of H3 residues 203−207 (Figure 2A). The unfolding of H3 enables the formation of β-bridges between stretches Thr191−Lys197 and Glu199−Thr204 (Figure 2B). The same set of residues is involved in β-structures in our present simulations of various constructs (WT (Figure 3B−E) and mutants (Figure 4B and C)) in two different force fields (GROMOS 43a1 and 53a6; Figure S4). Residues Thr191−Lys197 and Glu199−Thr204 had already been shown to form a β-seed when segment $H2H3^{182-217}$ was simulated under similar conditions.[4b] Although the Gromos force fields have been reported to favor β-sheets,[46] our results are in agreement with previous experimental and computational studies.

Previous mutagenesis experiments suggested that the detachment of H1 from the rest of the protein seems to be a key step in the conversion of PrP^C into PrP^{Sc}.[32,35] Indeed, in our simulations of $Cterm^{128-234}$, H1 showed an independent motion from the rest of the protein during the initial part of the simulation. The highly dynamic motion of H1 observed here is in agreement with the H1 displacement reported by van der Kamp and Daggett[15a] and De Simone et al.[14] Additionally, we showed here that H1 may act as an inhibitor of the conversion into the unfolded state leading to PrP^{Sc}. This inhibition involves the stabilization of the overall structure by

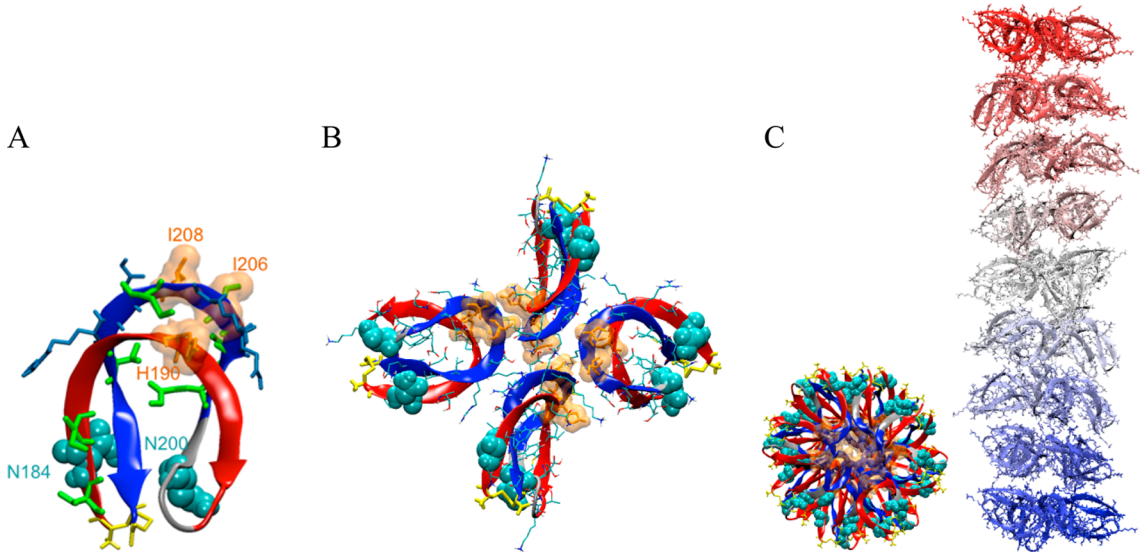

Figure 5. Model of H2H3 oligomerization. (A) β-rich H2H3$^{182-217}$ structure highlighting exposed residues 204−214 (blue liquorice) on H3 (dark blue). Hydrophobic patches identified by the water analysis are shown in green, glycosylation sites N184 and N200 in cyan, mutated residues affecting the oligomerization pathways in orange, and H2 residues in red. (B) Cartoon representation of the tetramer model based on interactions between residues 204−214 (blue). (C) Proposed model of the assembly of nine tetrameric units of H2H3$^{182-217}$ shown as top (left) and side (right) views.

strong hydrogen bonds between H1 and the H2H3 loop during the unfolding of H2H3. If H1 is deleted from the construct, the oligomerization profile of SEC remains identical to that of the full length OvPrP (Figure 3A). The simulation of the similar construct CtermΔH1 shows the persistence of β-bridges between Gln185−Thr195 and Gly198−Glu203 paralleled by the refolding of the loop between H2 and H3 toward the C-terminus (Figure 3B), a conformational pattern that has been previously observed in simulations of the H2H3 region 182−217 of OvPrP.[4b] In both simulations, a displacement of the native β-sheet S2 from the core of the protein was observed, suggesting that S2 may also protect H2H3 from unfolding and ultimately preventing the conversion to OvPrP^{Sc}. Campos et al.[36] observed *in silico* a strong conformational pH dependence of the human PrP^{c} conversion, with a decrease in helix content and an increase in β-sheet content at low pH. The main structural changes occurred in the helix-rich C-terminal core, in the regions around residues 135−155 and 185−200, corresponding to H1, to several residues of H2 and to the loop between H2 and H3. Khorvash et al.[9b] have used hydrogen exchange protection factors in restrained MD simulations to characterize long-time-scale fluctuations in human PrP^{C}. They observed that residues 182−194 corresponding to the last three turns of the H2 helix are lost in most structures and are partially replaced by β-strands (residues 183−192). These observations are in agreement with our findings, which show the conversion of the region between H2 and H3 into a β-rich structure.

Critical Residues for Multimerization. Our simulations of H2H3$^{175-229}$ and H2H3$^{182-217}$ show the unfolding of H2 followed by H3 as well as a high propensity for β-sheet formation along Gly192−Asp197 and Tyr199−Asn203, with the refolding of the newly formed β-sheet toward the C-terminus. These results are in agreement with previous results on the H2H3 construct spanning residues 182−217.[4b] H2 has already been reported as being more prone to unfolding than H3 by MD simulations.[12b,14,15] Another study by Lu et al. demonstrated by mass spectrometry and H/D exchange that the β-sheet core of the human PrP90−231 amyloid was formed by H2, a segment belonging to H3, and the H2H3 loop.[37] Recent NMR studies showed that residues 173−224 corresponding to H2, H3, and the N-terminal region of H2 with the NQNNF motif formed the core of Syrian hamster fibrils.[4c,38] Meli et al.[39] have observed that all 10 disease-associated mutations in their computational study produce dynamic changes which perturb the coordination of the H2−H3 hairpin. H2H3 has also been identified as the binding region for the antiprion compound GN8, which was shown to efficiently suppress local fluctuations by binding to flexible spots on H2 and to prevent mouse PrP urea-induced denaturation. GN8 has also been found to prolong the survival of TSE-infected mice by binding to the region connecting H2 (V189, T192, and K194) to the H2−H3 loop (E196) in mouse PrP by NMR and computer simulations. Similarly, Xu et al. have shown that poly-D-lysine, which removes proteinase K-resistant PrP from prion-infected SN56 neuroblastoma cells, binds to the PrP region containing H2 and H3. These results are all in good agreement with our observations of the critical role of H2 and H3 in the conversion of OvPrP.

To outline a molecular mechanism of the PrP^{C} conversion into the PrP^{Sc} form, we also analyzed mutant constructs, which were shown *in vitro* to dramatically affect oligomerization propensity and stability of the PrP^{C}. Several mutations on the human PrP^{C} structure are associated with diseases such as CJD[40] and Gerstmann−Straussler−Scheinker syndrome.[41] Susceptibility and resistance of sheep to scrapie have also been related to point mutations.[42] The property of single point mutants I206A and I208A to switch off the oligomerization of OvPrP underlines the importance of local changes in the conversion process. MD simulations of both constructs H2H3$^{182-217}$I206A and H2H3$^{182-217}$I208A showed a common tendency for H2 to unfold, as observed in WT constructs. However, while the I206A mutation prevented the unfolding of H3, I208A led to the refolding of the structure into a double β-hairpin without a stable β-sheet and with the formation of a new short helix from Gly198 to Glu203. We also observed that all WT constructs bent into a double β-hairpin in the same

region of H2 (Lys188 and His190) and H3 (Asp205 and Lys207), while the $H2H3^{182-217}$I208A mutant bent at Val187 and Val213. Thus, the unfolding of H2 and H3 occurring in the MD simulations appears to be critical to the conversion from $OvPrP^{C}$ to $OvPrP^{Sc}$. Fitzmaurice et al.[43] have correlated the ease of unwinding of H2 and H3 with the susceptibility of OvPrP variants to scrapie. It also appears from the results presented here that the refolding of H2H3 toward the C-terminus is a determinant of the oligomerization. As previously reported,[4b] the mutations H190A, I208M, and, as shown here, I206A and I208A, affect the oligomerization pathway. The fact that the point mutations are located in the "bending region" appears to be a critical element of the conversion process. This is supported by the observation that point mutation H190R (ovine H190 corresponds to human H187) is linked to Gerstmann–Straussler–Scheinker disease.[41]

A Model of Oligomerization. Fibrils formed by the yeast prion protein Sup35 were shown by X-ray crystallography to be formed by double β-sheets stacked in register, with side chains from two parallel β-sheets forming a dry interface closely bonding the β-sheets.[44] The hydrophobicity and water occupancy on the surface of $H2H3^{182-217}$ constructs suggest several residue patches that may be important for the oligomerization of OvPrP. On the other hand, our MD simulations and mutagenesis results imply a mechanistic role for the "bending region" in the conversion of $OvPrP^{C}$ to $OvPrP^{Sc}$. On the basis of this implication, we have created a tentative model for the assembly of OvPrP using $H2H3^{182-217}$ monomers (Figure 5A). Inferring from previous analyses, OvPrP oligomers O1, O2, and O3 are believed to be 12-, 24-, and 36-mers, respectively.[32] Consequently, the elementary building block of OvPrP oligomers can be based on either a trimer or a tetramer. We based our model on interactions involving residues 204–214 situated in the H3 bending region, because these residues are more exposed than H2 residues. This region also carries residues with a low water occupancy rate (T204, I206, I208, and V212) as identified in this paper, supporting its potential role in the oligomerization. Our attempt to build a trimer did not succeed in combining all constraints previously identified (Figure S6). Although we do not exclude the trimer hypothesis, we present here a tentative oligomer model based on a tetramer (Figure 5B), which was constructed using ZDOCK[31] and rigid body transformation, where nine units of tetramers were assembled along the fibril axis (Figure 5C). The ZDOCK program was selected because it has been shown to be particularly successful in predicting protein–protein interaction complexes.[31] Unlike the β-helix models previously proposed,[16b] our model only involves H2 and H3 residues, which were shown to be essential for oligomerization.[4b] Our findings are very much in line with recent REMD simulations on the C-terminal region of the prion suggesting that precursors of oligomeric states are characterized by a C-terminal β-rich core.[45] By comparing available experimental data of PrP protofibrils, DeMarco et al.[46] concluded that the β-helix model was not entirely reconcilable with several of the experimental observables. Therefore, the search of other models that can reconcile different sources of experimental data is still open. Here, we propose a model based on the tetramerization of single unfolded species based on exposed hydrophobic patches. Mereghetti and Wade[47] reported the tetramerization of hydrophobin proteins by MD simulations, where the interaction between units was mediated by nonpolar interactions between residues in the hydrophobic patch of the protein. These residues are located in hinges between β-sheets and rich in Ile and Val residues. The arrangement proposed for hydrophobin is strongly reminiscent of the arrangement proposed here for the oligomer of the β-rich H2H3 intermediate. We note that our oligomer model is not the only feasible structural arrangement of multiple H2H3 units, but it is the most plausible configuration given our current knowledge and recent results. Other regions of the OvPrP are likely to play a complementary role to H2H3 in a "dock and lock" amyloidogenic process and cytotoxity.

Summarizing, our work contributes mechanistic insights into the possible early conversion of $OvPrP^{C}$ into $OvPrP^{Sc}$. It is now clear that the destabilization of H2 and its unfolding are essential elements of the conversion mechanism. This conformational rearrangement of H2 is accompanied by the displacement of helix H1 and the native β-sheet S1, which uncover the hydrophobic core of the folded domain, enabling the complete unfolding of H3, followed by the formation of a β-sheet between residues from H2 and H3. The β-sheet refolds toward the C-terminus, exposing residues originally buried within the core. On the basis of water occupancy analysis and mutagenesis, we propose that the bending region (the "hinge") formed by residues 204–214 of H3 is at the origin of prion oligomerization. This mechanism should allow for structure-based design of oligomerization inhibitors using the H2H3 domain as a model for OvPrP.

■ ASSOCIATED CONTENT

Ⓢ Supporting Information

General scheme of the simulations performed (S1). Distance and H bonds analysis in the simulations of $Cterm^{128-234}$ and CtermΔH1 (S2). Table of energy decomposition for the simulated OvPrP constructs (S3). Secondary structure evolution of $Cterm^{128-234\text{-}restr}$ and S1H1S2 and snapshot structures of $H2H3^{182-217}$ replicas (S4). H bonds evolution in hydrogen bonds between residues 210 and 206 time evolution for the simulation of $H2H3^{182-217}$ and $H2H3^{182-217}$I206A (S5). Trimer model of $H2H3^{182-217}$ (S7). This material is available free of charge via the Internet at http://pubs.acs.org.

■ AUTHOR INFORMATION

Corresponding Author

*E-mail franca.fraternali@kcl.ac.uk.

Funding Sources

This work was funded by EPSRC/Diamond Light Source (CASE/CNA/07/31) (N.C., C.A.D.), the MRC National Institute for Medical Research (U11758331) (JK) and the Leverhulme Trust (F/07 040/AL) (FF, AF).

Notes

The authors declare no competing financial interest.

■ ACKNOWLEDGMENTS

Simulations were performed on the supercomputer MareNostrum at the Barcelona Supercomputing Center - Centro Nacional de Supercomputación (The Spanish National Supercomputing Center).

■ REFERENCES

(1) Prusiner, S. B. Prions. *Proc. Natl. Acad. Sci. U. S. A.* **1998**, *95*, 13363–83.

(2) Stahl, N.; Borchelt, D. R.; Hsiao, K.; Prusiner, S. B. Scrapie Prion Protein Contains a Phosphatidylinositol Glycolipid. *Cell* **1987**, *51*, 229−40.
(3) Riek, R.; Wider, G.; Billeter, M.; Hornemann, S.; Glockshuber, R.; Wuthrich, K. Prion protein NMR structure and familial human spongiform encephalopathies. *Proc. Natl. Acad. Sci. U. S. A.* **1998**, *95*, 11667−72.
(4) (a) Adrover, M.; Pauwels, K.; Prigent, S.; de Chiara, C.; Xu, Z.; Chapuis, C.; Pastore, A.; Rezaei, H. Prion Fibrillization Is Mediated by a Native Structural Element That Comprises Helices H2 and H3. *J. Biol. Chem.* **2010**, *285*, 21004−12. (b) Chakroun, N.; Prigent, S.; Dreiss, C. A.; Noinville, S.; Chapuis, C.; Fraternali, F.; Rezaei, H. The oligomerization properties of prion protein are restricted to the H2H3 domain. *FASEB J.* **2010**, *24*, 3222−31. (c) Tycko, R.; Savtchenko, R.; Ostapchenko, V. G.; Makarava, N.; Baskakov, I. V. The alpha-Helical C-Terminal Domain of Full-Length Recombinant PrP Converts to an In-Register Parallel beta-Sheet Structure in PrP Fibrils: Evidence from Solid State Nuclear Magnetic Resonance. *Biochemistry* **2010**, *49*, 9488−97.
(5) (a) Rigter, A.; Priem, J.; Timmers-Parohi, D.; Langeveld, J. P.; van Zijderveld, F. G.; Bossers, A. Prion protein self-peptides modulate prion interactions and conversion. *BMC Biochem.* **2009**, *10*, 29. (b) Yam, A. Y.; Gao, C. M.; Wang, X.; Wu, P.; Peretz, D. The octarepeat region of the prion protein is conformationally altered in PrP(Sc). *PLoS One* **2010**, *5*, e9316. (c) Frankenfield, K. N.; Powers, E. T.; Kelly, J. W. Influence of the N-terminal domain on the aggregation properties of the prion protein. *Protein Sci.* **2005**, *14*, 2154−66.
(6) Shmerling, D.; Hegyi, I.; Fischer, M.; Blattler, T.; Brandner, S.; Gotz, J.; Rulicke, T.; Flechsig, E.; Cozzio, A.; von Mering, C.; Hangartner, C.; Aguzzi, A.; Weissmann, C. Expression of amino-terminally truncated PrP in the mouse leading to ataxia and specific cerebellar lesions. *Cell* **1998**, *93*, 203−14.
(7) Dima, R. I.; Thirumalai, D. Exploring the propensities of helices in PrP(C) to form beta sheet using NMR structures and sequence alignments. *Biophys. J.* **2002**, *83*, 1268−80.
(8) Xu, Z.; Prigent, S.; Deslys, J. P.; Rezaei, H. Dual conformation of H2H3 domain of prion protein in mammalian cells. *J. Biol. Chem.* **2011**, *286*, 40060−8.
(9) (a) Gu, W.; Wang, T.; Zhu, J.; Shi, Y.; Liu, H. Molecular dynamics simulation of the unfolding of the human prion protein domain under low pH and high temperature conditions. *Biophys. Chem.* **2003**, *104*, 79−94. (b) Khorvash, M.; Lamour, G.; Gsponer, J. Long-time scale fluctuations of human prion protein determined by restrained MD simulations. *Biochemistry* **2011**, *50*, 10192−4.
(10) DeMarco, M. L.; Daggett, V. Characterization of cell-surface prion protein relative to its recombinant analogue: insights from molecular dynamics simulations of diglycosylated, membrane-bound human prion protein. *J. Neurochem.* **2009**, *109*, 60−73.
(11) Langella, E.; Improta, R.; Barone, V. Checking the pH-induced conformational transition of prion protein by molecular dynamics simulations: effect of protonation of histidine residues. *Biophys. J.* **2004**, *87*, 3623−32.
(12) (a) Colacino, S.; Tiana, G.; Broglia, R. A.; Colombo, G. The determinants of stability in the human prion protein: insights into folding and misfolding from the analysis of the change in the stabilization energy distribution in different conditions. *Proteins* **2006**, *62*, 698−707. (b) Blinov, N.; Berjanskii, M.; Wishart, D. S.; Stepanova, M. Structural domains and main-chain flexibility in prion proteins. *Biochemistry* **2009**, *48*, 1488−97.
(13) Chebaro, Y.; Derreumaux, P. The Conversion of Helix H2 to beta-Sheet Is Accelerated in the Monomer and Dimer of the Prion Protein upon T183A Mutation. *J. Phys. Chem. B* **2009**, *113*, 6942−8.
(14) De Simone, A.; Zagari, A.; Derreumaux, P. Structural and hydration properties of the partially unfolded states of the prion protein. *Biophys. J.* **2007**, *93*, 1284−92.
(15) (a) van der Kamp, M. W.; Daggett, V. Influence of pH on the Human Prion Protein: Insights into the Early Steps of Misfolding. *Biophys. J.* **2010**, *99*, 2289−98. (b) van der Kamp, M. W.; Daggett, V. Pathogenic mutations in the hydrophobic core of the human prion protein can promote structural instability and misfolding. *J. Mol. Biol.* **2010**, *404*, 732−48.
(16) (a) Wille, H.; Michelitsch, M. D.; Guenebaut, V.; Supattapone, S.; Serban, A.; Cohen, F. E.; Agard, D. A.; Prusiner, S. B. Structural studies of the scrapie prion protein by electron crystallography. *Proc. Natl. Acad. Sci. U. S. A.* **2002**, *99*, 3563−8. (b) Govaerts, C.; Wille, H.; Prusiner, S. B.; Cohen, F. E. Evidence for assembly of prions with left-handed beta-helices into trimers. *Proc. Natl. Acad. Sci. U. S. A.* **2004**, *101*, 8342−7.
(17) Rezaei, H.; Eghiaian, F.; Perez, J.; Doublet, B.; Choiset, Y.; Haertle, T.; Grosclaude, J. Sequential generation of two structurally distinct ovine prion protein soluble oligomers displaying different biochemical reactivities. *J. Mol. Biol.* **2005**, *347*, 665−79.
(18) Haire, L. F.; Whyte, S. M.; Vasisht, N.; Gill, A. C.; Verma, C.; Dodson, E. J.; Dodson, G. G.; Bayley, P. M. The crystal structure of the globular domain of sheep prion protein. *J. Mol. Biol.* **2004**, *336*, 1175−83.
(19) Berendsen, H. J. C.; van der Spoel, D.; van Drunen, R. Gromacs: A message-passing parallel Molecular Dynamics implementation. *Comput. Phys. Commun.* **1994**, *91*, 43−56.
(20) van Gunsteren, W. F.; Billeter, S. R.; Eising, A. A.; Huenenberger, P. H.; Krueger, P.; Mark, A. E.; Scott, W. R. P.; Tironi, I. G. *Biomolecular Simulation: The GROMOS96 Manual and User Guide*; Hochschulverlag AG: Zuerich, Switzerland, 1996.
(21) Oostenbrink, C.; Villa, A.; Mark, A. E.; van Gunsteren, W. F. A biomolecular force field based on the free enthalpy of hydration and solvation: the GROMOS force-field parameter sets 53A5 and 53A6. *J. Comput. Chem.* **2004**, *25*, 1656−76.
(22) Darden, T.; York, D.; Pedersen, L. Particle Mesh Ewald - an N.Log(N) Method for Ewald Sums in Large Systems. *J. Chem. Phys.* **1993**, *98*, 10089−92.
(23) Berendsen, H. P.; van Gusteren, J. P. M.; Hermans, W. F. J Interaction models for water in relation to protein hydration. *Intermol. Forces* **1981**, 331−42.
(24) van Gunsteren, W. F.; Berendsen, H. J. Computer simulation as a tool for tracing the conformational differences between proteins in solution and in the crystalline state. *J. Mol. Biol.* **1984**, *176*, 559−64.
(25) Kabsch, W.; Sander, C. Dictionary of Protein Secondary Structure - Pattern-Recognition of Hydrogen-Bonded and Geometrical Features. *Biopolymers* **1983**, *22*, 2577−637.
(26) Barrett, C. P.; Noble, M. E. Dynamite extended: two new services to simplify protein dynamic analysis. *Bioinformatics* **2005**, *21*, 3174−5.
(27) Cavallo, L.; Kleinjung, J.; Fraternali, F. POPS: A fast algorithm for solvent accessible surface areas at atomic and residue level. *Nucleic Acids Res.* **2003**, *31*, 3364−6.
(28) Fornili, A.; Autore, F.; Chakroun, N.; Martinez, P.; Fraternali, F. Protein-water interactions in MD simulations: POPS/POPSCOMP solvent accessibility analysis, solvation forces and hydration sites. *Methods Mol. Biol.* **2012**, *819*, 375−92.
(29) Daura, X.; Gademann, K.; Jaun, B.; Seebach, D.; van Gunsteren, W. F.; Mark, A. E. Peptide folding: When simulation meets experiment. *Angew. Chem., Int. Ed.* **1999**, *38*, 236−40.
(30) De Simone, A.; Dodson, G. G.; Verma, C. S.; Zagari, A.; Fraternali, F. Prion and water: tight and dynamical hydration sites have a key role in structural stability. *Proc. Natl. Acad. Sci. U. S. A.* **2005**, *102*, 7535−40.
(31) Chen, R.; Li, L.; Weng, Z. ZDOCK: an initial-stage protein-docking algorithm. *Proteins* **2003**, *52*, 80−7.
(32) Eghiaian, F.; Daubenfeld, T.; Quenet, Y.; van Audenhaege, M.; Bouin, A. P.; van der Rest, G.; Grosclaude, J.; Rezaei, H. Diversity in prion protein oligomerization pathways results from domain expansion as revealed by hydrogen/deuterium exchange and disulfide linkage. *Proc. Natl. Acad. Sci. U. S. A.* **2007**, *104*, 7414−19.
(33) Levitt, M. Conformational Preferences of Amino-Acids in Globular Proteins. *Biochemistry* **1978**, *17*, 4277−84.
(34) Chich, J. F.; Chapuis, C.; Henry, C.; Vidic, J.; Rezaei, H.; Noinville, S. Vesicle permeabilization by purified soluble oligomers of

prion protein: a comparative study of the interaction of oligomers and monomers with lipid membranes. *J. Mol. Biol.* **2010**, *397*, 1017−30.
(35) Hafner-Bratkovic, I.; Bester, R.; Pristovsek, P.; Gaedtke, L.; Veranic, P.; Gaspersic, J.; Mancek-Keber, M.; Avbelj, M.; Polymenidou, M.; Julius, C.; Aguzzi, A.; Vorberg, I.; Jerala, R. Globular domain of the prion protein needs to be unlocked by domain swapping to support prion protein conversion. *J. Biol. Chem.* **2011**, *286*, 12149−56.
(36) Campos, S. R. R.; Machuqueiro, M.; Baptista, A. M. Constant-pH Molecular Dynamics Simulations Reveal a beta-Rich Form of the Human Prion Protein. *J. Phys. Chem. B* **2010**, *114*, 12692−700.
(37) Lu, X.; Wintrode, P. L.; Surewicz, W. K. Beta-sheet core of human prion protein amyloid fibrils as determined by hydrogen/deuterium exchange. *Proc. Natl. Acad. Sci. U. S. A.* **2007**, *104*, 1510−5.
(38) Bjorndahl, T. C.; Zhou, G. P.; Liu, X.; Perez-Pineiro, R.; Semenchenko, V.; Saleem, F.; Acharya, S.; Bujold, A.; Sobsey, C. A.; Wishart, D. S. Detailed biophysical characterization of the acid-induced PrP(c) to PrP(beta) conversion process. *Biochemistry* **2011**, *50*, 1162−73.
(39) Meli, M.; Gasset, M.; Colombo, G. Dynamic diagnosis of familial prion diseases supports the beta2-alpha2 loop as a universal interference target. *PLoS One* **2011**, *6*, e19093.
(40) Peoc'h, K.; Manivet, P.; Beaudry, P.; Attane, F.; Besson, G.; Hannequin, D.; Delasnerie-Laupretre, N.; Laplanche, J. L. Identification of three novel mutations (E196K, V203I, E211Q) in the prion protein gene (PRNP) in inherited prion diseases with Creutzfeldt-Jakob disease phenotype. *Hum. Mutat.* **2000**, *15*, 482.
(41) Cervenakova, L.; Buetefisch, C.; Lee, H. S.; Taller, I.; Stone, G.; Gibbs, C. J., Jr.; Brown, P.; Hallett, M.; Goldfarb, L. G. Novel PRNP sequence variant associated with familial encephalopathy. *Am. J. Med. Genet.* **1999**, *88*, 653−6.
(42) Bruce, M. E. Scrapie strain variation and mutation. *Br. Med. Bull.* **1993**, *49*, 822−38.
(43) Fitzmaurice, T. J.; Burke, D. F.; Hopkins, L.; Yang, S. J.; Yu, S. L.; Sy, M. S.; Thackray, A. M.; Bujdoso, R. The stability and aggregation of ovine prion protein associated with classical and atypical scrapie correlates with the ease of unwinding of helix-2. *Biochem. J.* **2008**, *409*, 367−75.
(44) Nelson, R.; Sawaya, M. R.; Balbirnie, M.; Madsen, A. O.; Riekel, C.; Grothe, R.; Eisenberg, D. Structure of the cross-beta spine of amyloid-like fibrils. *Nature* **2005**, *435*, 773−8.
(45) Baillod, P.; Garrec, J.; Colombo, M. C.; Tavernelli, I.; Rothlisberger, U. Enhanced Sampling Molecular Dynamics Identifies PrP(Sc) Structures Harboring a C-Terminal beta-Core. *Biochemistry* **2012**, *51*, 9891−9.
(46) DeMarco, M. L.; Silveira, J.; Caughey, B.; Daggett, V. Structural properties of prion protein protofibrils and fibrils: an experimental assessment of atomic models. *Biochemistry* **2006**, *45*, 15573−82.
(47) Mereghetti, P.; Wade, R. C. Diffusion of hydrophobin proteins in solution and interactions with a graphite surface. *BMC Biophys.* **2011**, *4*, 9.